Laterally and Mutually Constrained Inversion of Surface Wave Seismic Data and Resistivity Data

Roger Wisén[1] and Anders V. Christiansen[2]
[1]Department of Engineering Geology, Lund University, Box 118, S-221 00 Lund, Sweden
Email: roger.wisen@tg.lth.se
[2]HydroGeophysics Group, Department of Earth Sciences, University of Aarhus,
Finlandsgade 8, DK-8200 Aarhus N, Denmark
Email: anders.vest@geo.au.dk

ABSTRACT

The laterally and mutually constrained inversion (LCI and MCI) techniques allow for the combined inversion of multiple geophysical datasets and provide a sensitivity analysis of all model parameters. The LCI and MCI work with few-layered models, and are restricted to quasi-layered geological environments. LCI is used successfully for inversion of surface wave (SW) seismic data and MCI for combined inversion of SW data and continuous vertical electrical sounding (CVES) data. The primary model parameters are resistivity or shear wave velocity and thickness, and depth to layer interfaces is included as a secondary model parameter.

The advantages and limitations of LCI and MCI are evaluated on synthetic SW data. The main conclusions are: Depth to a high velocity halfspace is generally well-resolved even if thicknesses of overlaying layers and the velocity of the halfspace are unresolved; Applying lateral constraints (LCI) between individual SW soundings improves model resolution, particularly for velocities and depths, and; Adding mutual constraints (MCI) to resistivity data improves model resolution of all parameters in the shear wave velocity model. When applied to field data, model resolution improves significantly when LCI or MCI is used, and resistivity and velocity models correlate structurally with better correlation to lithological interfaces identified in drill logs.

Introduction

Inversion of geophysical data is most often the last step in the interpretation for a geophysical model. The inverted model can be interpreted directly for the physical features that it describes which is not the case for the measured data. However, the inverted model has limitations that are important to acknowledge. Data collection is time consuming and it is often impossible to obtain the data quality that is needed to resolve a given physical model. Geophysical data, and surface wave seismic data in particular, are by nature insufficient, inconsistent and inaccurate (Jackson, 1972). Therefore, the geophysical model may have problems with hidden or suppressed layers, non-uniqueness, equivalence and lack of resolution in parts of the model.

Two ways to get an improved estimate of the inverted model are use of a priori information in the inversion and combined or joint inversion of different datasets. The use of good quality a priori information has been shown to be a successful approach (*e.g.,* Jackson, 1979; Wisén *et al.,* 2005). When more than one geophysical dataset is available, joint or combined inversion is an option. Examples of joint inversion of different combinations of geophysical data with different common model parameters have been presented earlier by Vozoff and Jupp (1975), Schmutz *et al.* (2000), Hertrich and Yaramanci (2002) and Christiansen *et al.* (2004). Examples of joint inversion combining seismic and DC resistivity methods include: Underground vertical seismic profiling (VSP) and DC resistivity (Dobroka *et al.,* 1991); Continuous VES (CVES) and seismic travel times (Gallardo and Meju, 2004), and; Refraction seismic and VES (Kis, 2002). In Hering *et al.* (1995) basic ideas for a joint inversion algorithm for VES and surface wave (SW) seismic data are presented, and in Misiek *et al.* (1997) two applications of this inversion algorithm are presented. Comina *et al.* (2002) also present joint inversion of VES and SW data based on the work of Hering *et al.* (1995) and Misiek *et al.* (1997). A fundamental assumption of joint VES and SW inversion methods are that the electrical and elastic interfaces are coincident, that is, the layer parameters have some kind of linear relationship.

We present a combined inversion of CVES and SW seismic data using a layered model description with lateral constraints. We use the layered and laterally constrained inversion scheme (LCI) presented by Auken and Christiansen (2004) as a base for a mutually constrained inversion (MCI) between the two data types. The seismic shear wave velocity models are coupled to each other with lateral

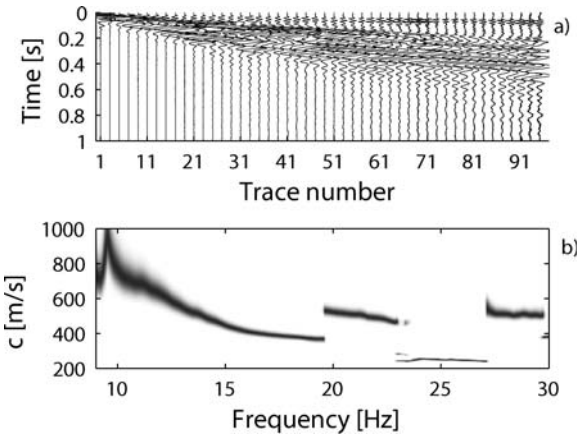

Figure 1. A 96-channel shot gather from a seismic survey. (a) t-x domain. The distance between traces is 1 m. Only odd-numbered traces are plotted. (b) f-c domain. The fundamental mode is identified from 10–19.5 Hz. Higher modes are also present at higher frequencies.

constraints on layer shear wave velocities and depths to layer interfaces. Likewise the resistivity models are coupled to each other with constraints on layer resistivities and depths to layer interfaces. Hereafter, LCI implies that a set of resistivity or surface wave data are inverted independently with lateral constraints, and MCI implies coupled inversion of the two datasets with lateral and mutual constraints.

With this inversion technique it is possible to invert the SW data using a layered model description incorporating a priori information. It also provides a full sensitivity analysis enabling quantitative evaluation of all model parameters. The method works with few-layered models, and is restricted to quasi-layered geological environments. The advantages and drawbacks of the combined inversion are examined through a thorough analysis of a range of synthetic models. Finally, the combined inversion is applied to a field dataset from a site investigation where a large number of geotechnical drill logs are available for verification of the results.

Surface Wave Method

In seismic methods the propagation of a wavefield is observed in order to characterize mechanical properties of the ground. Surface wave methods (SWMs) generally utilize the dispersive nature of Rayleigh waves in a layered medium to obtain a shear wave velocity (V_s) profile. Surface wave methods have been under development for several decades, and a thorough and up to date description of the available techniques is found in Socco and Strobbia (2004).

Data Processing

In this study the wavefield, measured in time and space (t-x) domain using a multi-station technique (*e.g.,* Park *et al.,* 1999; Foti, 2000), is transformed into frequency and phase-velocity (f-c) domain. In the f-c domain the energy distribution and dispersion of body and surface wave events can be analyzed. In this study only the fundamental mode dispersion curve, assumed to be dependent only on the Rayleigh wave, is extracted. The wavefield transformation of field data has been performed using the multi-channel analysis of surface waves (MASW) technique (Park *et al.,* 1999). The wavefield transformation and dispersion curve extraction comprise the processing of the SW data. Difficulties in extracting the fundamental mode dispersion curve can in some cases prevent this approach from functioning satisfactorily. Multi-modal observation and modeling (*e.g.,* Beaty and Schmitt, 2003), full wavefield modeling for inversion of either the f-c image (Forbriger, 2003a, b; Rydén, 2004) or effective dispersion curve (O'Neill, 2003) can overcome the restriction to a purely fundamental-mode assumption, but are not considered in this study. In Fig. 1, an example of a shot gather is presented in both t-x domain (Fig. 1a) and f-c domain (Fig. 1b).

Forward Response

Theoretical dispersion curves for a layered elastic medium can be calculated with a matrix formulation based on wave propagation theory. In this study, the stiffness matrix method proposed by Kausel and Roesset (1981) is used. Each layer is represented with a stiffness matrix where loads and displacements are expressed as a function of the material properties; Poisson's ratio (σ), V_s, thickness (t), density (ρ) of each layer, and the Rayleigh wave properties; radial frequency (ω) and c. By satisfying the boundary conditions at each layer interface, all layer matrices are assembled to a system matrix (**S**) describing the complete layer model. Each point on a dispersion curve is a function of ω and c and represents a solution to **S** where all boundary conditions are satisfied simultaneously. For modal solutions to exist **S** must be singular, *i.e.,* its determinant must be zero.

Discussion

Data collection and data processing are two parts of the investigation with large influence on data quality. These parts have not been investigated in this study. The impact on the final result from changes in σ and ρ are very small, less than 5% (Nazarian, 1984) compared to the impact from changes in V_s, and therefore σ and ρ are treated as fixed model parameters in the inversion. In all modeling performed in this study σ equals 0.4 and ρ equals 2 g/cm^3. These figures are based on results from geotechnical investigations performed in the field area.

Resistivity Method

DC resistivity measurements have been continuously developed for several decades and used with good results.

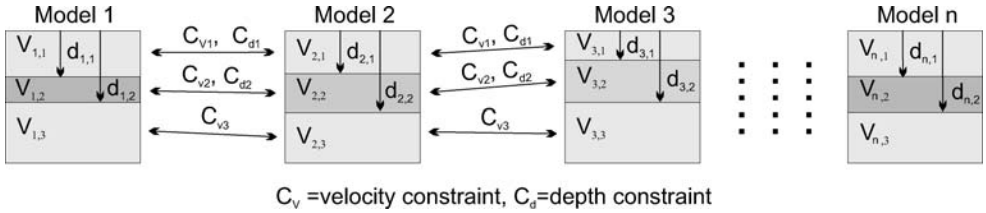

Figure 2. Schematic illustration of the LCI concept whereby 1D models are constrained laterally to create a section.

Continuous profiling to obtain a 2D image of the subsurface resistivity variation is a well-documented method (*e.g.,* Griffiths and Turnbull, 1985; Overmeeren and Ritsema, 1988), based on the fact that different geological materials have different electrical resistivities. Resistivity measurements have many different applications, both environmental and engineering (*e.g.,* Dahlin, 1996; Pellerin, 2002).

Data Collection

In order to obtain good resolution in the inverted model a high data density is an important factor. Modern resistivity measuring systems produce extensive datasets, and in this study resistivity data were collected as CVES data with a multi-electrode system (Dahlin, 1996).

Forward Response

In the 1D case used in this approach, forward responses are calculated as a summation of pole-pole responses over a layered earth as described by Telford *et al.* (1990). The potentials are computed using the Hankel transform filters of Johansen and Sørensen (1979) as calculated by Christensen (1990).

Inversion Methodology

The inversion methodology of the LCI is identical to that presented by Auken and Christiansen (2004). However, in this study two different data types and two different physical model descriptions are used.

Independent, unconstrained inversion of two datasets produces two uncorrelated models. Joint inversion implies that two related datasets are used in the same objective function, and one model is produced through the optimization process (Vozoff and Jupp, 1975). The laterally and mutually constrained inversion, presented here, optimizes two (or more) separate models that are geometrically constrained. Thus, it falls between the independent inversion and the joint inversion.

Laterally and Mutually Constrained Inversion

The term "constrained inversion" has previously been used when a concept or a priori data constrains the inversion. The term "laterally constrained inversion" (LCI) is here used for inverting data along a profile by minimizing a common objective function (Auken *et al.,* 2004). Hence, the LCI is a parameterized inversion of data of the same type with lateral constraints on the model parameters between neighboring models. The lateral constraints can be considered as a priori information on the geological variability within the investigated area; the smaller the expected variation of a model parameter, the more rigid the constraint. The resulting model section is laterally smooth with sharp layer interfaces as depicted in Fig. 2.

The term "mutually constrained inversion" (MCI) is used to describe the process in which two or more datasets with different geophysical properties and/or sensitivities, such as SW data and CVES data, are inverted. The MCI produces the same number of models as there are datasets, with a correlation between the models established through equality constraints between corresponding parameters as outlined in Fig. 3. Conversely, in joint inversion, *e.g.,* as presented in Hering *et al.* (1995), a common objective function is minimized resulting in just one inverse model. Thus, the MCI scheme offers a hybrid between individual and joint inversion. MCI allows the interpreter to incorporate the difference between the sensitivities of the contributing

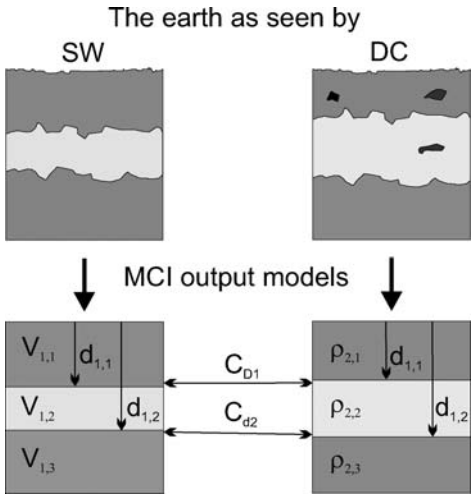

Figure 3. Schematic illustration of the MCI model concept, where different data types are connected via constraints on the model parameters.

datasets. The MCI was originally developed to combine electromagnetic and DC resistivity data, but because of the soft bounds between the two models, the approach is quite robust and can be used in a general approach.

In this paper we apply the LCI concept to the SW data. Also, we combine the LCI and the MCI concept to SW profile data and CVES data. The SW and CVES datasets are internally connected with lateral constraints to form a chain along the profile. The SW-LCI chain is then connected to the CVES-LCI chain through mutual constraints from individual shear wave velocity models to resistivity models. Hence, information from the SW data migrates to the CVES models and vice versa.

Since both methods provide information on depth to layers, the set of model parameters will be better resolved. Hidden or suppressed layers can be resolved, and ambiguity in solutions from potential methods, such as DC resistivity, can be reduced. If the depths to layer boundaries (which is the common model parameter and assumed to be the same in the two models) in reality disagree, there will be an error in one or both of the solutions. This will, however, be evident in the residual error of the mutual constraints.

Linearized Optimization

A detailed description of the practical implementation of the constraints is given in Auken *et al*. (2004), of which this is a short summary. The primary model parameters of the inversion scheme are layer resistivities, velocities and thicknesses. Depths to layer boundaries are included as secondary model parameters because constraints on depths are often preferred over constraints on thicknesses.

The dependence of the physical parameters of the subsurface is generally described as a non-linear, differentiable forward mapping. We use a linearized approximation by the first term of the Taylor expansion

$$\mathbf{d}_{obs} \cong \mathbf{g}(\mathbf{m}_{ref}) + \mathbf{G}(\mathbf{m}_{true} - \mathbf{m}_{ref}) + \mathbf{e}_{obs}, \qquad (1)$$

where $\mathbf{g}$ is the non-linear mapping of the model to the data space, $\mathbf{d}_{obs}$ and $\mathbf{e}_{obs}$ is the error on the observed data. The true model, $\mathbf{m}_{true}$, has to be sufficiently close to some arbitrary reference model, $\mathbf{m}_{ref}$, for the linear approximation to be valid. The Jacobian matrix, $\mathbf{G}$, contains the partial derivatives of the mapping

$$G_{st} = \frac{\partial d_s}{\partial m_t} = \frac{\partial \log(d_s)}{\partial \log(m_t)} = \frac{m_t}{d_s}\frac{\partial d_s}{\partial m_t}. \qquad (2)$$

The logarithm ensures positivity of the data and the model parameters (Johansen, 1977; Ward and Hohmann, 1988); however, operating in the logarithmic model space complicates the calculation of derivatives with respect to depths because the sum of thicknesses no longer translates to depth. We refer to Auken and Christiansen (2004) for the full derivation.

The constraints are connected to the true model by

$$\mathbf{R}\delta\mathbf{m}_{true} = \delta\mathbf{r} + \mathbf{e}_r, \qquad (3)$$

where $\mathbf{e}_r$ is the error on the constraints with 0 as the expected value, and $\delta\mathbf{r} = -\mathbf{R}\mathbf{m}_{ref}$ claims identity between the parameters tied by constraints in the roughening matrix, $\mathbf{R}$, containing 1 and −1 for the constrained parameters and 0 in all other places. The covariance matrix, $\mathbf{C}_R$, describes the strength, or variance, of the constraints. In the LCI approach we only operate with lateral constraints. In the MCI approach vertical constraints are also used in order to constrain the number of layers in the shear wave velocity model to a lesser number than in the resistivity model.

Rearranging equation (1) and combining it with equation (3) we write the inversion problem as

$$\begin{bmatrix}\mathbf{G}\\ \mathbf{R}\end{bmatrix}\cdot\delta\mathbf{m}_{true} = \begin{bmatrix}\delta\mathbf{d}_{obs}\\ \delta\mathbf{r}\end{bmatrix} + \begin{bmatrix}\mathbf{e}_{obs}\\ \mathbf{e}_{\mathbf{r}}\end{bmatrix}, \qquad (4)$$

or more compactly

$$\mathbf{G}'\cdot\delta\mathbf{m}_{true} = \delta\mathbf{d}' + \mathbf{e}'. \qquad (5)$$

If a priori data are used to constrain the inversion another row is added to equation (4). The covariance matrix for the joint observation error, e′, becomes

$$\mathbf{C}' = \begin{bmatrix}\mathbf{C}_{obs} & \underline{\underline{0}}\\ \underline{\underline{0}} & \mathbf{C}_R\end{bmatrix}. \qquad (6)$$

where $\mathbf{C}_{obs}$ is the covariance matrix for the observational error, $\mathbf{e}_{obs}$.

The model estimate

$$\delta\mathbf{m}_{est} = (\mathbf{G}'^T\mathbf{C}'^{-1}\mathbf{G}')^{-1}\mathbf{G}'^T\mathbf{C}'^{-1}\delta\mathbf{d}', \qquad (7)$$

minimizes

$$Q = \left(\frac{1}{N+A}[(\delta\mathbf{d}'^T\mathbf{C}'^{-1}\delta\mathbf{d}')]\right)^{\frac{1}{2}}, \qquad (8)$$

where A is the number of constraints and N is the number of data (Menke, 1989).

All datasets are inverted simultaneously, minimizing a common objective function, and the number of output models is equal to the number of 1D soundings. The constraints and the data are part of the inversion. Consequently, the output models form a balance between the constraints, the physics and the data. Model parameters with little influence on the data will be controlled by the constraints and vice versa. Information from one model will spread to neighboring models through the lateral and mutual constraints.

Constraints

In this study we combine two different geophysical methods with very different sampling density, as shown schematically in Fig. 4a. For each 1D sounding we have

a 1D model. The constraints between the models are based on the following three points:

1. Every DC model is constrained to its nearest neighboring DC models in both directions. Similarly, every SW model is constrained to its neighboring models on each side. This is illustrated in Fig. 4b.
2. The neighboring SW and the DC models are constrained to each other, as illustrated in Fig. 4c.
3. All lateral constraints, C_l, are scaled according to the model separation, d, using

$$C_l = C_r\sqrt{\frac{d}{d_r}} \tag{9}$$

where C_r is a reference constraint for the reference distance, d_r. Therefore, if the distance between two constrained models is twice that of the reference distance, the constraint values between the two models are multiplied by a factor of $\sqrt{2}$, which is a less tight constraint.

Combining the constraints applied in above points 1 and 2 yields the full set of constraints as sketched in Fig. 4(d). In the case of just one data type (*e.g.,* LCI on SW data) only points 1 and 3 are applied.

In these examples we used reference constraints, C_r, of 0.1 on resistivities and velocities and 2 m on depths, except depth to bedrock which was set to 1 m (this is due to a much smaller expected variation of this depth). The mutual constraint was 2 m on all depths to allow for geometrical differences in the resistivity and shear wave velocity models. The reference distance, d_r, is 4 m, reflecting the sounding distance employed for the CVES data. This means that layer resistivity and velocity are allowed to vary approximately 10% and interface depths by at least $\pm$ 1 m over a distance of 4 m.

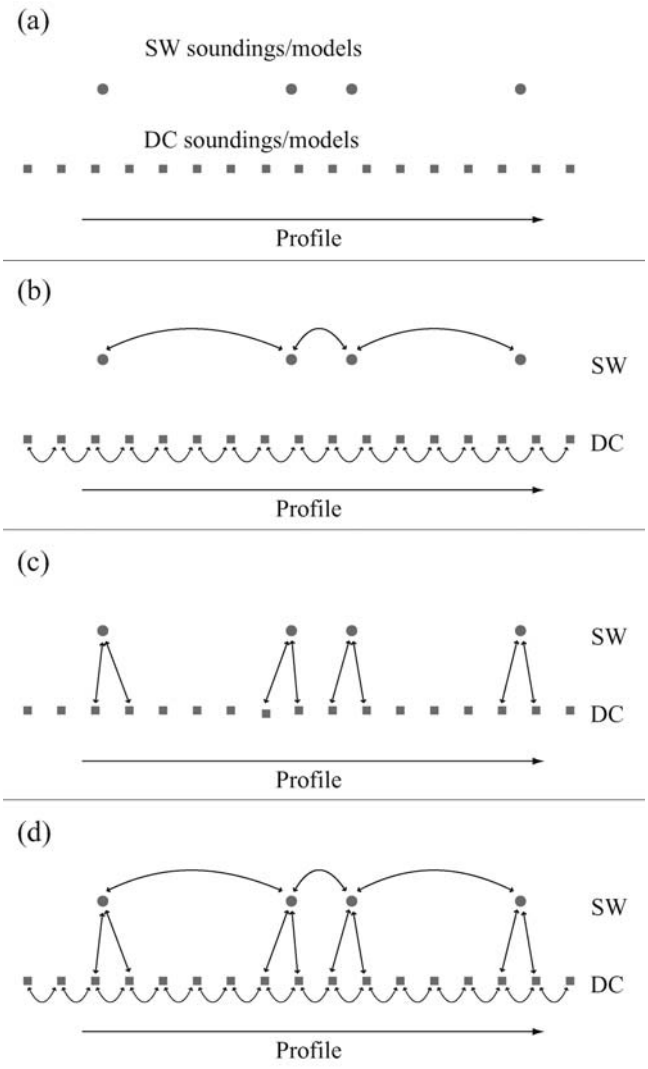

Figure 4. Schematic illustration of lateral and mutual model constraints indicated by arrows: (a) A simplified sketch of the distribution of SW and DC soundings and their corresponding models, (b) lateral constraints internally between the DC and internally between the SW are applied, (c) mutual constraints between the DC and SW are applied, and (d) a summary of the total set of constraints.

Analysis of Model Estimation Uncertainty

The sensitivity analysis of model parameters can be used to assess the resolution of the inverted model. The parameter sensitivity analysis of the final model is the linearized approximation of the covariance of the estimation error, C_{est}, (Tarantola and Valette, 1982):

$$\mathbf{C}_{est} = (\mathbf{G}'^{T}\mathbf{C}'\mathbf{G}')^{-1}. \tag{10}$$

Standard deviations on model parameters are calculated as the square root of the diagonal elements in $\mathbf{C}_{est}$. Because the model parameters are represented as logarithms, the analysis gives a standard deviation factor (STDF) on the parameter m_s that is defined by

$$STDF(m_s) = \exp\left(\sqrt{C_{est,ss}}\right). \tag{11}$$

Thus, the theoretical case of perfect resolution has a STDF = 1. We define well-resolved parameters to have a STDF $<$ 1.2, which is approximately equivalent to an error of 20%, moderately resolved parameters fall within 1.2 $<$ STDF $<$ 1.5, poorly resolved parameters 1.5 $<$ STDF $<$ 2, and unresolved parameters have a STDF $>$ 2.

Discussion

The CVES dataset (and thus inverted model) is positioned according to the lateral focus points of the various electrode configurations. For symmetric configurations the lateral focus point is equal to the center of the array. Similarly, in multi-channel phase velocity analysis,

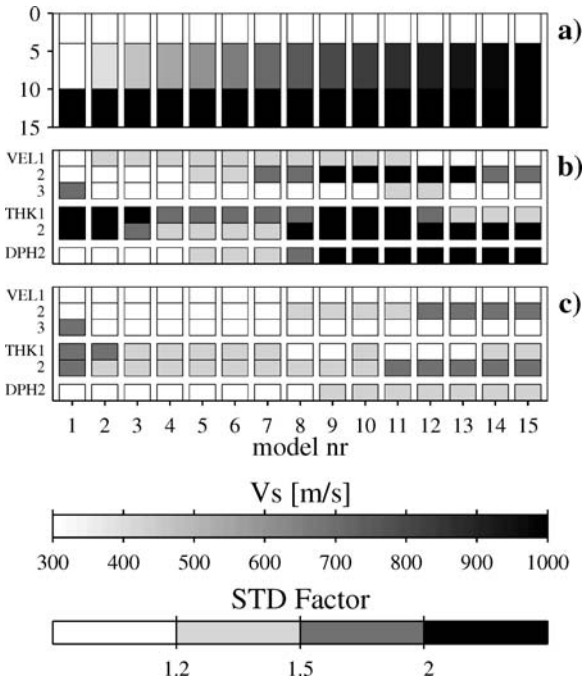

Figure 5. Models and results from the synthetic resolution study: (a) Fifteen 3-layer models with gradual increase in velocity of layer two, (b) sensitivity analysis of the models in (a), and (c) sensitivity analysis of the models in (a) when MCI with a resistivity dataset is used.

the dispersion curve represents the average response under the recording array. For both methods the corresponding plane parallel layered model for inversion is arbitrarily positioned at the center of the recording spread. In "roll-along" surveys, the shot spacing is usually much smaller than the spread length, thus there is a large degree of propagation path overlap. Lateral geological variations strictly void both 1D surface wave and resistivity inversion. However, relatively gentle dips can be imaged in a "smeared" fashion, depending on the degree of overlap. The laterally constrained inversion scheme is quite robust and handles this systematic error well.

Synthetic Resolution Study

To better understand the SW model resolution and how LCI and MCI affect the SW model resolution a synthetic resolution study was performed. This test is performed as the parameter sensitivity analysis presented in equations (10) and (11). It takes into account only the model and the size of the dataset and is not preceded by an actual inversion. All models used resemble the expected velocity model in the field study. The datasets used resemble typical datasets for a single sounding in the field study. The synthetic SW dataset has a frequency range of 11–30 Hz. This is the typical range within which reliable fundamental mode dispersion data have been measured in the field study presented in this paper. The single sounding DC dataset extracted from a full CVES dataset contains 53 data points with unique Schlumberger configurations and/or midpoints. This is the exact amount of data with midpoints in a 4 m interval along the measurement line as in the field study. For both datasets the standard deviation is set to 5%. The sensitivity analysis of individual parameters is presented as a four-graded gray scale ranging from well-resolved (white) to unresolved (black). The analysis presents sensitivities of shear wave velocities (V_s), thickness of layers (t) and depths to layer boundaries (d).

Resolution of an Intermediate Layer

The aim of this test was to investigate the resolution of intermediate layer boundaries and velocities. Figure 5a presents fifteen, 3-layer models where the shear wave velocity of layer 1, $V_{s,1}$, is equal to 300 m/s, $V_{s,2}$ is 300–1,000 m/s gradually changing in steps of 100 m/s, $V_{s,halfspace}$ is 1,000 m/s, the thickness of layer 1, t_1, is 4 m and t_2 is 6 m and hence the depth to halfspace, $d_{halfspace}$, is 10 m. The sensitivity analysis of this test, Fig. 5b, shows that $V_{s,1}$ and $V_{s,halfspace}$ is well resolved or resolved (white and light gray), and that $V_{s,2}$ is poorly resolved or unresolved (dark gray and black) except when it is very close to $V_{s,1}$. The analysis also show that t_1 and t_2 are mostly unresolved but that $d_{halfspace}$ is well resolved or resolved as long as $V_{s,2}$ is not higher than 600 m/s. Figure 5c presents the sensitivity analysis of the model in Fig. 5a when MCI with resistivity data is used.

Resolution with Varying Depth to Halfspace

This test aimed to show how the resolution changes when $d_{halfspace}$ increases. Figure 6a presents nineteen, 2-layer models where $V_{s,1}$ is 300 m/s, $V_{s,halfspace}$ is 1,000 m/s and $d_{halfspace}$ is gradually increasing from 2 m to 20 m. The sensitivity analysis of this test, Fig. 6b, shows that $V_{s,1}$ is well resolved, except when $d_{halfspace}$ is 2 m where it is unresolved, $V_{halfspace}$ is well resolved or resolved as long as $d_{halfspace}$ is not greater than 10 m and finally that $d_{halfspace}$ is resolved or well resolved except when it equals 2 m.

Resolution with Varying Frequency Content

This test aimed to show how the resolution changes when the low frequency content of the SW data changes from f_{min} of 5 Hz to f_{min} of 15 Hz. For this study a two-layer model where $V_{s,1}$ is 300 m/s, $V_{s,halfspace}$ is 1,000 m/s and $d_{halfspace}$ is 12 m was used (model number 11 in Fig. 6b). The sensitivity analysis of this test, Fig. 7, shows that $V_{s,halfspace}$ is well resolved or resolved for f_{min} equal to 9 Hz or lower and that $d_{halfspace}$ is well resolved or resolved for the entire frequency range.

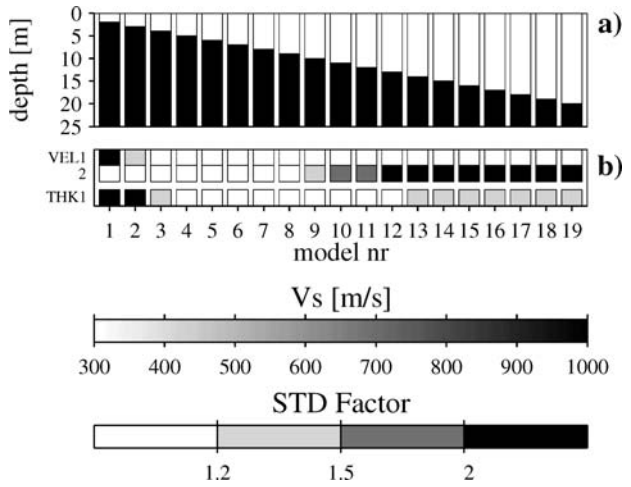

Figure 6. Models and results from the synthetic resolution study: (a) Nineteen 2-layer models with an increasing thickness of layer one, and (b) sensitivity analysis of the models in (a).

Resolution with Mutual Constraints to CVES Data

The last test aimed to show how MCI with CVES data affect the resolution of the velocity model. For this study the velocity models in Fig. 5a is coupled to a resistivity model through constraint on depths. The resistivity in the model layer 1, R_1, is 50 Ωm, R_2 is 25 Ωm, $R_{halfspace}$ is 150 Ωm and the thicknesses are the same as in the velocity model. The sensitivity analysis of this test, Fig. 5c, shows that the resolution of $V_{s,1}$, $V_{s,2}$, t_1, t_2 and $d_{halfspace}$ is significantly improved. The effect on the resistivity model resolution is not considered in this study.

Discussion

Conclusions that can be drawn from these synthetic studies are that:

(i) Depth to halfspace is generally well-resolved, even when the lowest available frequency increases and/or depths to halfspace increase;
(ii) Resolution of the halfspace shear wave velocity decreases when the low frequency content in the SW data decreases and/or when the depth to halfspace increase;
(iii) the shear wave velocity and thickness of the intermediate layer in a three-layer model is generally poorly resolved but the velocity is resolved as long as it is close to or only slightly higher than the velocity of the top layer;
(iv) Individual thicknesses are generally poorly resolved and;
(v) MCI with CVES data generally improves the model resolution. This is valid for all model parameters, even velocities that are not directly coupled.

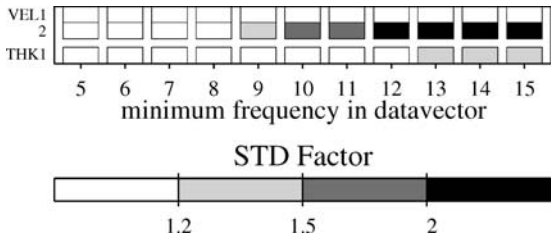

Figure 7. Models and results from the synthetic resolution study: sensitivity analysis of 11 reproductions of model 11 in Fig. 6a using 11 different datasets with lowest frequency ranging from 5 Hz until 15 Hz.

The depth to a boundary can be well resolved without the individual overlying thicknesses being well-resolved, in fact it will often be the case in models where a high-contrast boundary is below one or more low-contrast boundaries. In this study that is the case for a high-velocity layer covered by two or more layers with lower velocity. An equivalent example is a low-resistivity layer covered by two or more high-resistivity layers mapped by an electromagnetic method (Danielsen *et al.,* 2003).

The low sensitivity of intermediate layers imposes that the number of layers should be kept as low as possible without violating the data fit. For the analysis to be valid the residual error should be kept lower than the standard deviation of the data. Since thicknesses are generally poorly resolved it is important to note that the inversion also includes depth as a secondary model parameter. The fact that depth to the high-velocity halfspace is well-resolved in most conditions is positive. Even without low frequency content in the SW data and/or with halfspace depth of up to (or possibly above) 20 m a good estimate of the depth to halfspace is achieved.

Case Study

The case study presented here is from the City Tunnel Project (CTP) in the city of Malmö in southern Sweden. The seismic data were collected on two occasions (2001 and 2004) in order to evaluate the SWM. The resistivity data were collected as part of the site investigation for a railway connection to CTP. The geological environment consists of 10–15 m of glacial deposits underlain by limestone. The glacial deposits can be subdivided into two separate clay tills with an embedded sandy and/or silty layer of inter-morainic sediments that exist in parts of the field area. Near the surface post-glacial coarse-grained sediments can be found.

Field Procedures and Model Parameterization

The seismic survey was performed with a 24-channel seismograph and 4.5 Hz geophones, either coupled to the

ground by spikes or mounted on heavy steel plates connected by a wire and pulled by a vehicle. Geophone spacing was 1 m. Based on the assumption of reciprocity between source and receivers, 48–96 channels were simulated with a walk-away approach. In practice the source was moved an array length away from the geophones instead of moving the geophones. A number of 24-channel shot gathers were then concatenated to give a simulated larger dataset. The source consisted of a sledgehammer impacting on a steel plate for better coupling. The aim was to collect a dataset that consists of a number of seismic "soundings" along a measuring line. The sounding spacing differs along the line but was in general 10 m. For most datasets 48 channels were used for analysis.

The resistivity survey was performed with a multi-electrode "roll-along" system. Minimum electrode distance is 2 m, maximum electrode distance 148 m and the electrode configuration was a combination of Wenner and Schlumberger.

The seismic dataset contains 21 separate dispersion curves with different profile coordinates. The lowest frequency of the fundamental mode varies from 9–22 Hz with an average of 11.5 Hz and the upper limit of the frequency varies from 13–55 Hz with an average of 25 Hz. A standard deviation of 5% was assumed for all frequencies. O'Neill (2003) show that the standard deviation is frequency dependent with smaller errors at high frequencies and larger errors at low frequencies, compared with what is assumed here. Since only one seismogram was recorded for each measurement point it was not possible to estimate the standard deviation of the data in this field study.

For the seismic model four layers were used. A three-layer model did not allow the data to fit and a five-layer model was found to be poorly resolved. For the resistivity model five layers were used. For the MCI it is necessary to have an equal number of model parameters (depths to layer boundaries) to constrain between the resistivity and velocity models respectively. Thus, an equal number of layers in the resistivity and velocity models are required. Here, both the resistivity and velocity models have 5-layers. However, the seismic model was effectively re-parameterized to four layers (which is the number of layers used for the independent inversion and LCI) by very tightly constraining the velocities between layers three and four. In practice, this regularization is achieved with a vertical constraint, as mentioned in the inversion methodology section (above). The standard deviation between the layer velocities is set to zero percent, which makes the velocities in these two layers equal. Elsewhere, the constraints used are the same as described in the inversion methodology section (above); layer resistivity and velocity are allowed to vary approximately 10% and interface depths by at least $\pm$ 1 m over a distance of 4 m.

Independent Inversion and LCI

Figure 8a presents the resulting V_s models after independent inversion on all SW data with the sensitivity analysis of model parameters in Fig. 8b and the normalized data misfits in Fig. 8c. The normalized data misfit is 1 if the data are fit at the assumed observational error of 5% and smaller for a smaller misfit. The model in Fig. 8a shows $V_{s,halfspace}$ ranging from 800–1,800 m/s and $d_{halfspace}$ ranging from 8–21 m. Figure 8b shows that very few model parameters are resolved. The normalized data misfit in Fig. 8c is around 0.5 for all soundings which is well below the assumed observational error.

Figure 8d presents the resulting V_s model after LCI on all SW data, Fig. 8e presents the accompanying resolution analysis of model parameters and Fig. 8f presents the normalized data misfit for each dataset. In Fig. 8d lithology from drill logs has been added for comparison. In the drill logs, white represents sorted sediments, dark grey represents clay till and light grey represents limestone. The model in Fig. 8d shows $V_{s,halfspace}$ ranging from 850–1,650 m/s and $d_{halfspace}$ ranging from 10–17 m. Most model parameters, including all velocities and depths, are well-resolved or resolved. Only thicknesses are generally poorly resolved or unresolved. The normalized data misfit is only slightly higher than for the independent inversion and still well below the observational error.

The effect of performing LCI instead of independent inversion can be seen clearly directly in the model, Fig. 8d. The model parameters are now much more consistent along the measuring profile. The resolution of the model parameters (Fig. 8e) is dramatically improved. In particular velocities and depths are improved. The alternative ways to improve model resolution while employing a single surface wave mode would be to use a model with fewer layers or to use many more layers with fixed thickness and soft vertical constraints between layer velocities. The first alternative would not fit the data for most dispersion curves and hence only be useful for a very small part of the data. The second alternative would result in a smooth model without physical resemblance to the sedimentary layered geology that is present. Of course, incorporating higher modes and/or broader frequency ranges would also assist, but this study was restricted to the fundamental mode only.

MCI

Finally, the information from the CVES data is combined with the SW data to see if it is possible to improve the SW models by adding more information on the thickness of layers and depths to interfaces. The result is shown in Fig. 9. Figure 9a presents the resulting V_s and resistivity model after MCI on all SW and CVES data. Figure 9b presents the resolution analysis of the seismic model parameters and Fig. 9c presents the normalized data misfit for each SW dataset. Since there is about 5–10 times

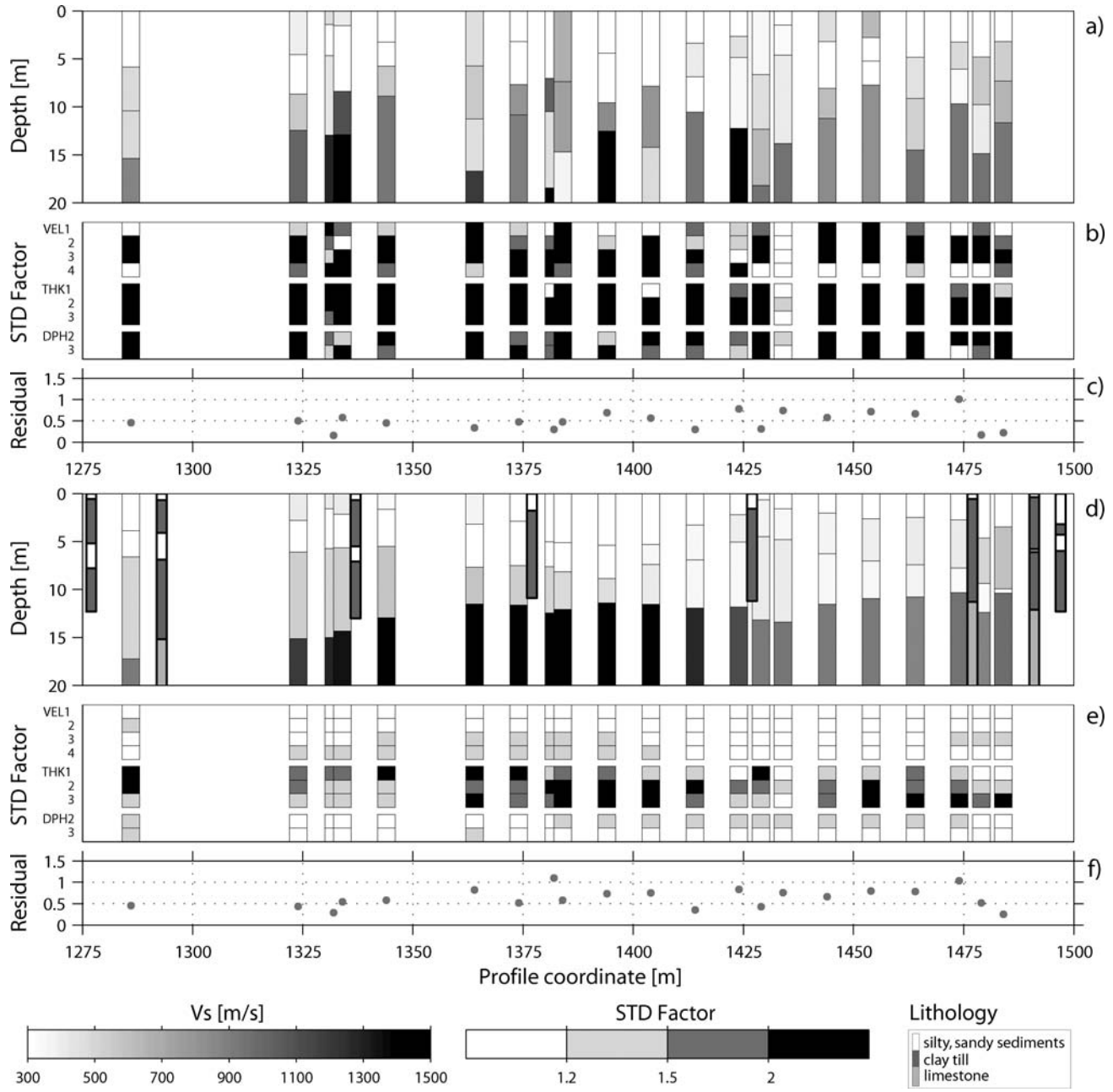

Figure 8. Result from inversion of SW data: (a) V_s model from independent inversion on all SW data, (b) model resolution analysis of the model in (a), (c) normalized data misfit presented for each dataset, (d) LCI on all SW data, (e) model resolution analysis of the model in (d), and (f) normalized data misfit presented for each dataset. In the LCI model lithology from drill logs is present. In the drill logs, white represents sorted sediments, dark grey represents clay till and light grey represents limestone.

more CVES resistivity data than SW data the impact of the seismic data on the resistivity model is very small. The resistivity model presented here was verified earlier (Wisén *et al.,* 2005) and will not be analyzed here. The V_s model in Fig. 9a shows $V_{s,halfspace}$ ranging from 800–1,450 m/s and $d_{halfspace}$ ranging from 9.5–13.5 m. Most model parameters, including all velocities, depths and most thicknesses are well-resolved or resolved. The normalized data misfit corresponding to the SW data is only slightly higher than for the independent inversion and actually lower than for the LCI on SW data alone. It is also well below the observational error.

The main difference between the V_s model in Fig. 9a and the model in Fig. 8d is on the analysis of the thickness

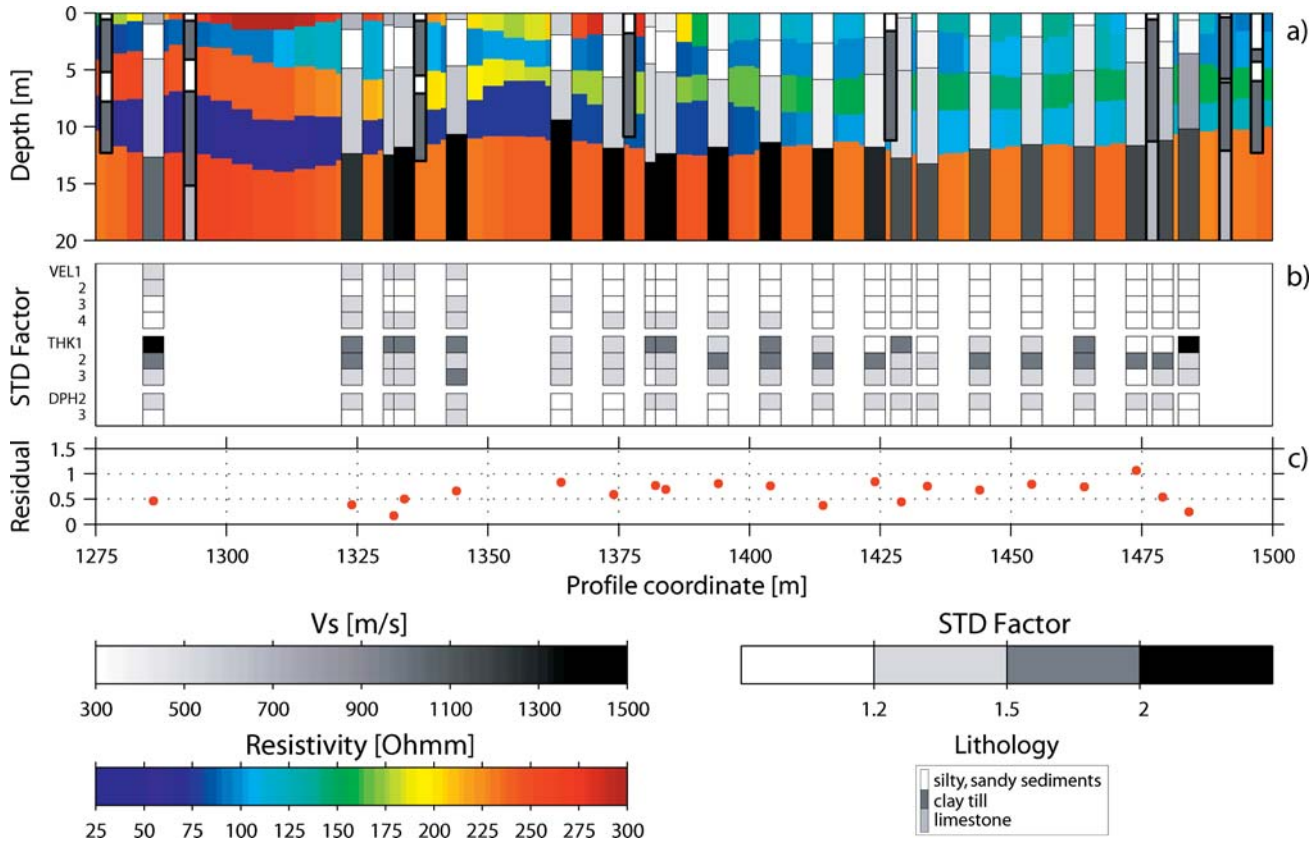

Figure 9. Results from combined inversion of SW and CVES data: (a) Resistivity (color) and V_s (grayscale) model after MCI, (b) model resolution analysis of the V_s model in (a), and (c) normalized data misfit presented for each dataset. In the LCI model lithology from drill logs is present. In the drill logs, white represents sorted sediments, dark grey represents clay till and light grey represents limestone.

and the variation of model parameters. Information on thickness of the high-resistivity top layer found in the CVES profile, helps constrain the shear wave velocity of that layer. The velocity of the halfspace also changed a bit as a result from additional information on the depth to the interface. Moreover, the geophysically interpreted interfaces correlate better with lithological interfaces identified in drill logs.

Figure 10 presents the measured data and model response for the model at profile coordinate 1,429 m. For this dataset the root mean square error is 1.6% for independent inversion, 2.1% for LCI and 2.2% for MCI. Combined, these model responses fit well within the expected observational error of 5%. The largest misfit occurs at the lowest frequency. At frequencies above 15 Hz the error seems to decrease with frequency. The model response from LCI and MCI agree well and both differ from the model response from independent inversion. This is due to influence from neighboring models through the lateral and mutual constraints. Even though the model resolution is improved in this case, it is not the new improved model that is the main benefit from performing MCI, but rather the knowledge that the resistivity model and the seismic model actually correspond geometrically. This information is very important and can be used in the geological and geotechnical interpretation of other resistivity data in this area.

Conclusions

Both laterally and mutually constrained inversion (LCI and MCI) is applied to both synthetic and field surface wave (SW) dispersion data and continuous vertical electrical sounding (CVES) data.

It is concluded from the synthetic study that the depth to a high-velocity homogenous halfspace below one or more overlying layers is well-resolved, more so than the shear wave velocity. This applies both for an increasing depth and a decreasing amount of low frequency content. The intermediate layer in a three-layer model is generally less resolved than that of the top layer and halfspace, unless the layer velocity is similar to the velocity in the top layer. Individual thicknesses of overburden layers are generally poorly resolved, and therefore it is important to note that the inversion also includes depth as a secondary model parameter. MCI with CVES data generally improves the

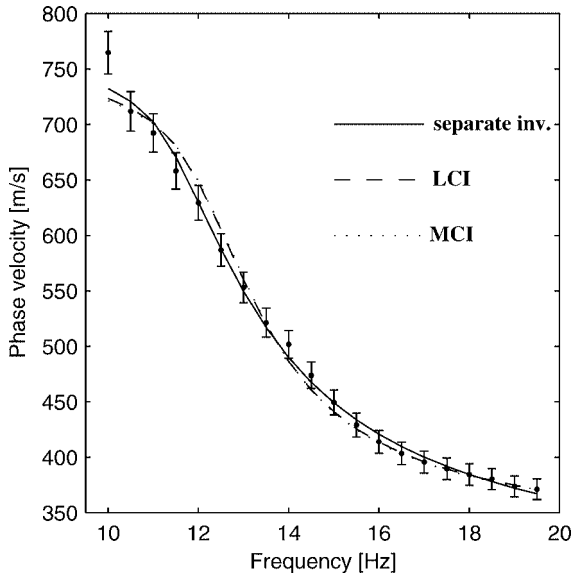

Figure 10. Observed data and model responses from the seismic model at profile coordinate 1,429 m.

model resolution. This is valid for all model parameters, even velocity, which is not directly coupled between the two model types.

From a field survey, independent inversion of the SW datasets gives models with a high degree of lateral variation along the measuring profile. The model parameters in a four-layer model are generally poorly resolved or unresolved. The data fit is good, about half that of the assumed observational error of 5%. Performing LCI instead of independent inversion makes the model evolve smoothly along the measuring profile without violating the data fit. The resolution of the model parameters is dramatically improved, in particular for velocities and depths. Performing MCI results in a slightly improved resolution of the shear wave velocity model. In particular the thicknesses are better resolved, and the geophysically interpreted interfaces correlate better with lithological interfaces identified in drill logs. The main benefit from performing MCI is the additional information on how the resistivity and velocity models share similar structural features, which greatly assists lithological interpretation.

Acknowledgments

We acknowledge: The City Tunnel Project for providing reference data and an interesting case; Mats Svensson, Tyréns AB, for being generous with equipment and time; Sven Tyréns foundation for funding a large part of the Ph.D. study of Roger Wisén; the Nordic Research Academy for funding visits for Roger Wisén to Aarhus university during which this project was initiated; Bo Holm-Jacobsen, Esben Auken, Nils Rydén, Torleif Dahlin and Mats Svensson for valuable comments during the work; Adam O'Neill and Sebastiano Foti for constructive reviews.

References

Auken, E., and Christiansen, A.V., 2004, Layered and laterally constrained 2D inversion of resistivity data: Geophysics, **69**, 752–761.

Auken, E., Christiansen, A.V., Jacobsen, B.H., Foged, N., and Sørensen, K.I., 2004, Piecewise 1D Laterally Constrained Inversion of resistivity data: Geophysical Prospecting, in press.

Beaty, K.S., and Schmitt, D.R., 2003, Repeatability of multimode Rayleigh-wave dispersion studies: Geophysics, **68**, 782–790.

Christensen, N.B., 1990, Optimized fast Hankel transform filters: Geophysical Prospecting, 1990, **38**, 545–568.

Christiansen, A.V., Auken, E., Foged, N., and Sørensen, K.I., 2004, Mutually and laterally constrained inversion of CVES and TEM data—A case study: Near Surface Geophysics, Submitted.

Comina, C., Foti, S., Sambuelli, L., Socco, L., and Strobbia, C., 2002, Joint inversion of VES and surface wave data: Proceedings of SAGEEP, Las Vegas, Nevada, 11 pp.

Dahlin, T., 1996, 2D resistivity surveying for environmental and engineering applications: First Break, **14(7)** 275–283.

Danielsen, J.E., Auken, E., Jørgensen, F., Søndergaard, V.H., and Sørensen, K.I., 2003, The application of the transient electromagnetic method in hydrogeophysical surveys: Journal of Applied Geophysics, **53**, 181–198.

Dobroka, M., Gyulai, A., Ormos, T., Csokas, J., and Dresen, L., 1991, Joint inversion algorithm of seismic and geoelectric data recorded in an underground coal mine: Geophysical Prospecting, **39**, 643–666.

Forbriger, T., 2003a, Inversion of shallow-seismic wavefields: I. Wavefield transformation: Geophysical Journal International, 2003, **153**, 719–734.

Forbriger, T., 2003b, Inversion of shallow-seismic wavefields: II. Inferring subsurface properties from wavefield transforms: Geophysical Journal International, 2003, **153**, 735–752.

Foti, S., 2000, Multistation methods for geotechnical characterization using surface waves: Ph.D. Dissertation, Politecnico di Torino.

Gallardo, L.A., and Meju, M.A., 2004, Joint two-dimensional dc resistivity and seismic traveltime inversion with cross-gradients constraints: Journal of Geophysical Research, **109**, B03311.

Griffiths, D.H., and Turnbull, J., 1985, A multi-electrode array for resistivity surveying: First Break, **3(7)** 16–20.

Hering, A., Misiek, R., Gyulai, A., Ormos, T., Dobroka, M., and Dresen, L., 1995, A joint inversion algorithm to process geoelectric and surface wave seismic data. Part I: Basic ideas: Geophysical Prospecting, 1995, **43**, 135–156.

Hertrich, M., and Yaramanci, U., 2002, Joint inversion of surface nuclear magnetic resonance and vertical electrical sounding: Journal of Applied Geophysics, **50**, 179–191.

Jackson, D.D., 1972, Interpretation of inaccurate, insuffient and inconsistent data: Geophysical Journal Of The Royal Astronomical Society, **28**, 97–109.

Jackson, D.D., 1979, The use of a priori data to resolve non-uniqueness in linear inversion: Geophysical Journal Of The Royal Astronomical Society, **57**, 137–157.

Johansen, H.K., 1977, A man/computer interpretation system for resistivity soundings over a horizontally stratified earth: Geophysical Prospecting, **25**, 667–691.

Johansen, H.K., and Sørensen, K.I., 1979, Fast Hankel transforms: Geophysical Prospecting, 1995, **27**, 876–901.

Kausel, E., and Roesset, J.M., 1981, Stiffness matrices for layered soils: Bulletin of the Seismological Journal of America, **71**, 1743–1761.

Kis, M., 2002, Generalised series expansion (GSE) used in DC geoelectric-seismic joint inversion: Journal of Applied Geophysics, **50**, 401–416.

Menke, W., 1989, Geophysical data analysis—discrete inverse theory: International Geophysics Series, Academic Press, San Diego.

Misiek, R., Liebig, A., Gyulai, A., Ormos, T., Dobroka, M. and Dresen, L., 1997, A joint inversion algorithm to process geoelectric and surface wave seismic data. Part II: Applications: Geophysical Prospecting, 1997, **45**, 65–85.

Nazarian, S., 1984, In situ determination of soil deposits and pavement systems by spectral analysis of surface waves method, Ph.D. thesis, University of Texas at Austin, Texas.

O'Neill, A., 2003, Full-waveform reflectivity for modelling, inversion and appraisal of seismic surface wave dispersion in shallow site investigation: Ph.D. thesis (unpublished), The University of Western Australia [http://earth.kumst.kyoto-u.ac.jp/~adam/].

Overmeeren, R.A. van, and Ritsema, I.L., 1988, Continuous vertical electrical sounding: First Break, **6(10)** 313–324.

Park, C.B., Miller, D.R., and Xia, J., 1999, Multichannel analysis of surface waves: Geophysics, **64**, 800–808.

Pellerin, L., 2002, Applications of electrical and electromagnetic methods for environmental and geotechnical investigations: Surveys in Geophysics, **23**, 101–132.

Rydén, N., 2004, Surface wave testing of pavements, Doctoral thesis, Lund, Sweden, ISBN: 91-973406-4-2.

Schmutz, M., Albouy, Y., Guérin, R., Maquaire, O., Vassal, J., Schott, J.J., and Descloitres, M., 2000, Joint electrical and time domain electromagnetism (TDEM) data inversion applied to the super sauze earthflow (France): Surveys in Geophysics, **21**, 371–390.

Socco, L.V., and Strobbia, C., 2004, Surface-wave method for near-surface characterization: A tutorial: Near Surface Geophysics, **2(4)** 165–185.

Tarantola, A., and Valette, B., 1982, Generalized nonlinear inverse problems solved using a least squares criterion: Reviews of Geophysics and Space Physics **20**, 219–232.

Telford, W.M., Geldart, L.P., and Sheriff, Robert E., 1990, Applied geophysics, 2nd ed. Cambridge University Press, Cambridge, England.

Vozoff, K., and Jupp, D.L.B., 1975, Joint inversion of geophysical data: Geophysical Journal of the Royal Astronomical Society, **42**, 977–991.

Ward, S.H., and Hohmann, G.W., 1988, Electromagnetic theory for geophysical applications: Electromagnetic Methods in Applied Geophysics, Vol. 1, (ed in M.N. Nabighian) pp. 131–311, SEG publication.

Wisén, R., Auken, E., and Dahlin, T., 2005, Combination of 1D Laterally Constrained Inversion and 2D smooth inversion of resistivity data with a priori data from boreholes: Near Surface Geophysics, **3(2)** 71–79.